Structures 34 (2021) 2628–2643

Contents lists available at ScienceDirect

Structures

journal homepage: www.elsevier.com/locate/structures

Local plate buckling type imperfections for NSS and HSS welded box-section columns

M. Radwan *, B. Kövesdi

Budapest University of Technology and Economics, Department of Structural Engineering, Műegyetem rkp. 3., 1111 Budapest, Hungary

ARTICLE INFO

Keywords:
Imperfections
Local buckling
Welded box-section
Stability design
High strength steel

ABSTRACT

The finite element model-based design of steel structures is getting increasing attention by designers, especially in the case of buckling problems of welded plated structures and by the static check of the interacting stability behaviour. The FEM-based design approach is introduced and standardised in the EN 1993–1-5 Annex C providing the ability to calculate the buckling resistance based on direct resistance check by geometrical and material non-linear analysis using imperfections (GMNIA). By this design process, the application of imperfections (shape and magnitude) has a large impact on the computed buckling resistance. It is especially true if the interacting stability phenomenon (interaction of plate and column-like behaviour) is to be analysed. The general way to consider imperfections in FE models is the application of equivalent geometric imperfections covering the effect of residual stresses and geometric imperfections. Several previous investigations prove the application of equivalent geometric imperfections can lead to conservative resistance, especially in the case of the interacting stability problem because the application of two different equivalent geometric imperfections leads to duplication of the residual stresses. Therefore, it is highly important to determine the appropriate imperfection shape and size for buckling problems. The current paper deals with the determination of local plate buckling-type imperfection, which can be further applied in numerical models used for interacting stability problems, which is the next step of the planned research program. Within the current paper, the necessary imperfection magnitudes are determined for welded square box-section columns for various steel grades (S235 – S960) to perfectly match the local buckling resistance proved by test results and gives design proposals for FEM-based design approaches.

1. Introduction

Slender plates having a large width-to-thickness ratio present a reliable solution for the different construction projects because of their lightweight that contributes to material saving and cost-effective design. This is especially true for products manufactured from high-strength steel (HSS: S500 – S960). In addition to the increased utilisation of conventional steel grades, also known as normal strength steel (NSS: S235 – S460), high strength steel (HSS) is becoming more popular recently due to its numerous advantages, such as lightweight and high load-bearing capacity. Different studies discussed the differences between normal strength steel and high strength steel structures, indicating many differences in the material properties and stability behaviour coming from the manufacturing and fabrication process. Therefore, it is highly important to develop more economical design rules supporting the design of slender steel girders manufactured from NSS or HSS. The current paper investigates the local buckling resistance of slender welded box-section columns, their FEM-based design approach and gives a design proposal for imperfection magnitudes to be used for a wide range of steel materials (S235 – S960) and plate slenderness ratios.

The current EN 1993–1-5 [1] standard provides a design method using analytical design equations to check the local buckling resistance to pure compression using the modified Winter-type curve as a plate buckling curve (denoted as Winter-type curve in further investigations). The equivalent geometric imperfection provided by the EN 1993–1-5 Annex C [1] has been calibrated to the Winter-type buckling curve, and an imperfection magnitude of $b/200$ is proposed in FEM-based design calculations, where b is the plate width. The same design rule has been taken over in the newest Eurocode provision, in prEN 1993–1-14 [2], which is currently under development.

However, the applicability of the EN 1993–1-5 based buckling curve

* Corresponding author.
E-mail address: mohammed.radwan@emk.bme.hu (M. Radwan).

https://doi.org/10.1016/j.istruc.2021.09.011
Received 21 May 2021; Received in revised form 1 September 2021; Accepted 4 September 2021
Available online 21 September 2021

has been criticised by several researchers in the past. It has been shown based on test results and detailed numerical investigations that the provided local buckling resistance is not on the safe side for square box-section columns, and a new buckling curve has been proposed to this special case. Details on the previous research results are given in [3–5]. Schillo et al., [4,15] proposed a new buckling curve or suggested using an increased partial safety factor for plate buckling resistance of plates subjected to pure compression. The proposed new buckling curve is extremely close to the buckling curve of EN 1993–1-5 Annex B [1] (denoted as Annex B curve in further investigations). Schillo et al. proved that the proposed new buckling curve fits the safety level of the EN 1990 [6] using the partial safety factors provided by EN 1993–1-5 [1]. Therefore, the application of this buckling curve has a strong theoretical and test-based background, which are also proved by numerical parametric study and detailed statistical evaluation. Within the current investigations, therefore, the Annex B curve is considered as a theoretically and experimentally proved buckling curve for the local buckling resistance of box-section columns.

It also means the standardised equivalent geometric imperfection for plate buckling needs revision because the buckling curve has been changed for this special case. Thus, the proposed and usually used imperfection magnitude b/200 refers to the Winter curve. A safety problem could arise if designers used b/200 as equivalent geometric imperfections in the design. This situation could give the impression to designers that FE calculation is more appropriate than the analytical approach, and it could give resistance increase as expected from the FEM-based design approaches. However, for this specific situation, this is not the case, and wrong imperfection magnitudes are applied in the FE model. Therefore, the aim of the current research work is to eliminate this safety-bypass issue and to draw attention, ensuring safe side results. The applied imperfection magnitude should be not equal to b/200 but a different value depending on the slenderness ratio of the plate.

The first focus of the current investigation is on the magnitude of the equivalent geometric imperfection fitting the buckling resistance to the Winter-type curve or Annex B curve, respectively. The current code also has shortcomings because magnitude only for the equivalent geometric imperfections is provided, and no specified appropriate value is given for the geometric imperfections if residual stresses are also applied in the numerical model. It was shown in previous studies [7,8] that these factors and their combinations have a significant effect on the ultimate buckling resistance. Therefore, the second focus of the current research program is on the determination of the necessary magnitude of geometric imperfections if predefined residual stress patterns are applied. This is highly important in the further analysis of box-section columns investigating local and global buckling interaction behaviour. For the previously mentioned reasons, the current study aims to find a suitable combination of imperfections and residual stresses to achieve an accurate estimation of the local buckling resistance for slender sections made of NSS and HSS under pure compression.

At first, the study started by creating a numerical model validated by test results available in the literature. With the numerical model, the buckling resistance is determined by geometrically and materially nonlinear analysis using imperfections (GMNIA). On the validated numerical model, a numerical parametric study is executed investigating the effect of imperfections on the buckling resistance. The imperfection sensitivity study has been executed twice for each analysed geometry using (i) equivalent geometric imperfections and (ii) geometric imperfections + residual stresses. The obtained buckling resistances are compared to the Winter-type curve and Annex B curve, and the necessary imperfection amplitudes are determined. The parametric study is executed within a wide parameter range for different slenderness ratios using six different steel grades (from S235 up to S960). As an additional outcome of the current research program, design proposals are developed for the imperfection magnitudes applicable in the FEM-based design of welded plated structures, which can also be used to determine the interaction resistance between global and local buckling.

The Winter-type curve or another standardised buckling curves, which have a test-based origin, consider manufacturing imperfections (geometrical imperfections and residual stresses) by their actual value and due to the scatter within the test results and statistical evaluation process to determine the characteristic resistance, the manufacturing uncertainties are considered correctly. However, this is not the case for the FEM-based design approach. Only if it is not a validation process supported by laboratory tests. In the numerical model, the designer should apply appropriate equivalent geometric imperfections or geometric imperfections and residual stresses, which magnitudes highly influence the buckling resistance. Therefore, these imperfections should have been validated for the basic physical phenomena, in this case, for buckling under pure compression. The current paper fits the lack of this imperfection calibration and validation process.

2. Literature review

2.1. Plate buckling resistance according to EN 1993–1-5 using modified Winter-type curve

In the EN 1993–1-1 [9], plates susceptible to local buckling are classified as cross-section class 4. Sections of class 4 cannot attain their elastic resistance and are characterised by local buckling failure. The design of such types of plates can be done by using the reduced stress method or using the effective width method of the EN 1993–1-5 [1]. The buckling behaviour of a plate under compression depends on the ratio of its principal dimensions, namely the plate length (*a*), width (*b*), and thickness (*t*). Because the plate elements in box-section columns are relatively thin compared to their width, when loaded in compression, they may buckle. The disposition of any plate parts within the cross-section may limit the axial load carrying capacity or the bending resistance of the section. If the plates are thin and plate buckling resistance limits the resistance of the cross-section, the Eurocode suggests calculating the effective area of the compression zone of the plates with a reduced (so-called effective) area based on the following equations. The effective area of the compression zone should be obtained by *Eq. (1)*.

$$A_{c,eff} = \rho \cdot A_c \tag{1}$$

where: ρ is the reduction factor for plate buckling,

A_c is the gross cross-sectional area.

The reduction factor (ρ) for internal compression elements may be taken by *Eqs. (2)-(4)*.

$$\rho = \begin{cases} 1, & \bar{\lambda}_p \le 0.5 + \sqrt{0.085 - 0.055\psi} \\ \dfrac{\bar{\lambda}_p - 0.005(3+\psi)}{\bar{\lambda}_p^2} \le 1, & \bar{\lambda}_p > 0.5 + \sqrt{0.085 - 0.055\psi} \end{cases} \tag{2}$$

$$\bar{\lambda}_P = \sqrt{\frac{f_y}{\sigma_{Cr}}} = \frac{\bar{b}/t}{28.4\varepsilon\sqrt{k_\sigma}} \tag{3}$$

where:

Ψ is the stress ratio,

$\bar{b}$ is the appropriate width to be taken as follows (Table 5.2 of EN 1993–1-1 [9])

$k_\sigma$is the buckling factor corresponding to the stress ratio Ψ and boundary conditions given in Table 4.1 or Table 4.2 of Eurocode [1],

t is the thickness of the plate,

σ_{Cr} is the elastic critical plate buckling stress,

ε is a yield strength dependent factor

$$\varepsilon = \sqrt{\frac{235}{f_y \left[\frac{N}{mm^2}\right]}} \tag{4}$$

This calculation method is widely used in design practice, and its applicability has been validated and proved by many researchers in the past.

2.2. Plate buckling resistance according to EN1993-1–5 using buckling curve of Annex-B

The reduced stress method is briefly covered in Section 10 of EN 1993–1-5 [1], as an alternative approach to the effective width method. In the current paper, this design method is not used. Therefore it will be not introduced in the details, only the provided buckling curve is given by the *Eqs. (5)-(7)*, which buckling curve is proved reliable and safe-sided for the plate buckling resistance calculation of square box-section columns.

$$\rho = \frac{1}{\phi_p + \sqrt{\phi_p^2 - \overline{\lambda}_\rho}} \tag{5}$$

$$\varphi_\rho = \frac{1}{2}\left(1 + \alpha_\rho\left(\overline{\lambda}_\rho - \overline{\lambda}_{p0}\right) + \overline{\lambda}_\rho\right) \tag{6}$$

$$\overline{\lambda}_p = \sqrt{\frac{\alpha_{ult,k}}{\alpha_{cr}}} \tag{7}$$

where: $\alpha_{ult,k}$ is the minimum load amplifier of the design loads to reach the characteristic resistance of the plate in the most critical point and α_{cr} is the minimum amplifier to reach the elastic critical load of the plate. The values of $\overline{\lambda}_{p0}$ and α_p are given in Table B.I of EN 1993–1-5 [1] where for the welded section with ψ greater than 0 these values are equal to 0.7 and 0.34, respectively.

2.3. Previous research results

Numerous experimental and numerical investigations are behind these standardised buckling curves. A short introduction is given in this section. Nishino et al., [10] tested four welded stub columns, two made of ASTM A7 (A36, $f_y = 250$ N/mm^2) steel, and two made of ASTM A514 (quenched and tempered, $f_y = 689$ N/mm^2) steel. The residual stresses and the buckling resistance were investigated within this research program. The results of experiments indicated that considerable post-buckling strength might be expected for elastic buckling of plates, although not for elastic–plastic buckling [10]. Dwight tested a set of 49 stub columns conducted at the Engineering Department in Cambridge. The study concluded that the buckling curve and the effective width suggested by Winter are unsafe. Therefore, the American and British Standard had changed in practice to lower reduction factors. The experimental results on the residual stresses of the welded box-section columns also proved the width of the tension area should be independent of the plate width above b/t ratio of 25 [11]. Rasmussen [12] conducted a test program on a box, cruciform, and I-section stub columns fabricated from BISALLOY 80 steel (Australian steel, equivalent to an ASTM A514, quenched and tempered), with a nominal yield strength of 690 MPa. Six box sections were investigated regarding their buckling strength with plate slenderness ranging from 0.4 to 0.7, comprising three different slenderness configurations with two repetitions for each. It was found that stocky plates are less affected by residual stresses than slender plates because the cross-section of a stocky plate is almost completely plastic at the ultimate load level. They found that the compressive residual stress magnitude decreases by increasing plate slenderness. Thus, strain hardening properties of high strength steel are inferior compared to normal strength steel. The non-dimensional strength of stocky HSS plates is smaller than that of stocky plates manufactured from NSS [12]. Bridge and O'Shea [13] executed local buckling tests on concrete-filled and not-filled steel stub-columns with a yield strength of $f_y = 282$ N/mm^2. The tests were performed to investigate the local buckling behaviour of short thin-walled square section columns with or without internal restraint. Two test series were performed to study the effect of the buckling mode and the influence of the specimen length. Based on the research results, it was concluded the British Standard gives a good approximation for the local buckling resistance in the case of slender plates while it is unconservative for thicker plates. Therefore, a modification of the Winter formula was proposed by the authors based on the obtained test results.

Clarin [8] executed an experimental research program on specimens made of S420, S700, and S1100 steel material. The investigated specimens were stub columns to prevent the global buckling with the height of specimens equal to three times the width. The nominal plate slenderness was altered in the test program between 0.7 and 1.5. In addition to the test results, a deep literature review was executed for both the plate buckling resistance and residual stress pattern of high-strength steel box sections. It was found by the author that the Winter-type curve needs more adjustment concerning slender plates with $\bar{\lambda}_p$ greater than 0.9 since in its current form overestimates the local buckling resistance as proved by test results. This observation indicates the need for further study of the local buckling behaviour of HSS columns. The author also concluded the absolute magnitude of tensile residual stresses in welded high strength steel plates is higher than for normal strength steel structures. However, its value is lower compared to the yield strength of each material.

Halme et al., [14] investigated 12 test specimens made of S960 steel grade. Specimens were manufactured by first milling two identical plates. These plates were then bent to form two L-shaped sections with sharp corners. Finally, the two sections were placed in a jig, and the corners were laser welded. The results confirmed the previous observation of researchers. The Eurocode buckling curve gives non-conservative reduction factors for slender sections, i.e., the calculated ultimate buckling loads are higher than obtained from the test results. A more refined reduction factor was proposed by the authors, showing a smaller reduction factor than proposed by the Winter-type curve. On the contrary, the proposed buckling curve is slightly conservative for plate slenderness between 0.673 and 0.9, and shows good agreement with the test results for the entire analysed parameter range.

Shi et al., [7] performed 13 welded stub-column tests made of S460 steel grade. The length of the column (L) was designed fitting to a local buckling half-wavelength correspond to all test specimens. Therefore, these columns were sufficiently compact to avoid overall buckling instabilities. Results showed the local buckling stress σ_{cr}, the ultimate stress σ_u, and the stress ratio σ_{cr}/σ_u decreased by the increase of the width-to-thickness ratios of plates (b/t), that is indicating that local buckling occurred before yielding of the plates. Additionally, the post-buckling strength increased as the width-to-thickness ratio increased. It was found that after applying suitable imperfections and residual stresses, FEM analyses could estimate the ultimate strength of the different sections accurately. After the comparison of the test results and FE calculations by the different codes, it was found that for box-section columns, the current design methods were not safe.

Schillo et al., [15] performed an extensive experimental research program on 34 tests made on a square welded box-section stub columns with large b/t ratios. Test specimens were made of S500, S700, and S960 steel grades by varying the plate slenderness between 0.64 and 1.55. Imperfection measurements were done with the aid of laser technology to have a three-dimensional image of imperfections for each face of the tested columns. The amplitude of the local imperfections is determined by using surface fitting. Based on the test results, it was found that for increasing local slenderness, the post-buckling behaviour becomes less pronounced, while for stocky sections, a sharper drop after reaching the ultimate load occurs. FEM model was developed and validated based on the test results, and it was used to conduct a numerical parametric study. It was noticed that the deviation of the experimental results from the theoretical resistance of the EN1993-1–5 increases by the relative slenderness ratio, while the tendency tends to more optimistic results. Therefore, the authors suggested a new approach that is claimed to be

more appropriate for the estimation of the local buckling resistance. With the aid of the available data from the experiments and numerical simulations, a new buckling curve was proposed fitting the experimental results to an exponential equation. It was also shown that the resistance function of the original Winter-type curve (developed by Kármán et al., [16] and modified by Winter [17]) could be improved regarding accuracy when the buckling curve is changed to an exponential equation. Schillo et al. collected all the internationally available test results regarding local buckling of steel box-section columns. Results of 114 stub-column tests are found, re-evaluated, and plotted on graphs against the local slenderness ratio. It has been noticed, many tests lie below the Winter-type curve, while the Annex B curve represents a better estimation of the test results. The applicability of the Annex B curve (or similar curve proposed by Schillo) has also been proved based on statistical evaluation and detailed safety assessment.

Based on the current literature review, it can be observed that many studies criticised the Winter-type curve and suggested that more detailed analyses should be carried out regarding the determination of the local buckling resistance. Previous research activities concluded that the Winter-type curve provides approximately the mean value of the test result and provides larger resistance than the characteristic value of the plate buckling resistance. It means that this buckling curve does not fit the safety requirement of EN 1990 [6], and it needs revision. Thus the Annex B curve is considered a good estimation of the characteristic buckling resistance. Therefore, within this study, this buckling curve is considered as an appropriate alternative to the Winter-type curve.

However, this change in the buckling curve has been not considered in the FEM-based design of steel structures. It means that the local buckling type imperfection also needs revision. The main aim of the current study is to find the appropriate equivalent geometric imperfections and combinations of residual stresses and geometric imperfections to be used in a numerical model, obtaining an ultimate buckling resistance equal to the result provided by the Annex B curve. Just for comparison purposes, the necessary imperfections to the Winter-type curve are also evaluated and introduced in the paper. Thus, there is a lack of information on the applicable imperfections leading to this lower buckling curve. The current investigations and their results provide crucial information to the FEM-based design of steel plated structures.

3. Description of the numerical model

3.1. Geometrical model, boundary conditions and imperfections

To investigate the structural behaviour of box-section columns having slender plates, a parametric numerical model is developed using the FE program ANSYS 17.2 [18]. The numerical model is a full shell model using four-node thin shell elements. The general layout of the numerical model and the used notations are shown in Fig. 1, presenting the geometrical model of the box-section column with the applied finite element mesh and the general shape of the applied imperfections with increased magnitudes for better visibility. The numerical model aims to investigate the structural behaviour and to determine the buckling resistance of welded box-section columns eliminating the effect of flexural (global) buckling. Therefore, the length of the analysed stub columns is set three times the width of the section.

Boundary conditions are chosen to represent a reliable estimation of the pure local buckling resistance having pinned supports. The boundary conditions of the model are assigned on two master nodes placed in the centre of gravity of the end cross-sections. Restrictions of the translational movements are set on both nodes, leaving one node free to move in the direction of the loading. Rigid diaphragms are defined at the two end cross-sections using rigid members linking all the 6 DOFs between the master node and the cross-section nodes. At one end of the segment, the centre of gravity of the cross-section is restrained against translations (UX, UY, UZ) and rotation in the Z-direction (ROTZ). At another end, only two translational DOFs (UX, UY) and the rotation in the Z-direction (ROTZ) are restrained, and compressive force acting in the centre of gravity of the cross-section is applied in the longitudinal direction (FZ).

The mesh size is selected to obtain accurate estimations of the structural behaviour. The number of the applied finite elements along the width of the plates is also harmonised with the geometry of the applied residual stress pattern to ensure the correct application of the residual stresses as well. A mesh sensitivity study has been executed for the smallest and largest plate width studied in the current analysis, and one example is presented in Fig. 2. The applied mesh size is governed by the width of the cross-section. Every single plate consists of at least 8 finite elements within one cross-section. Therefore, the assigned mesh

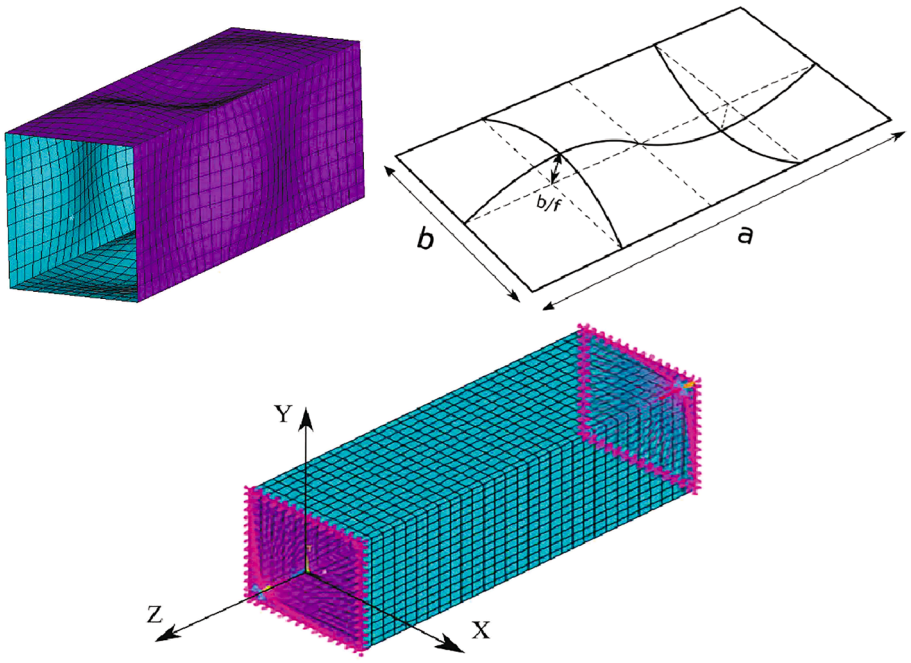

Fig. 1. Geometrical model, applied imperfections and boundary conditions.

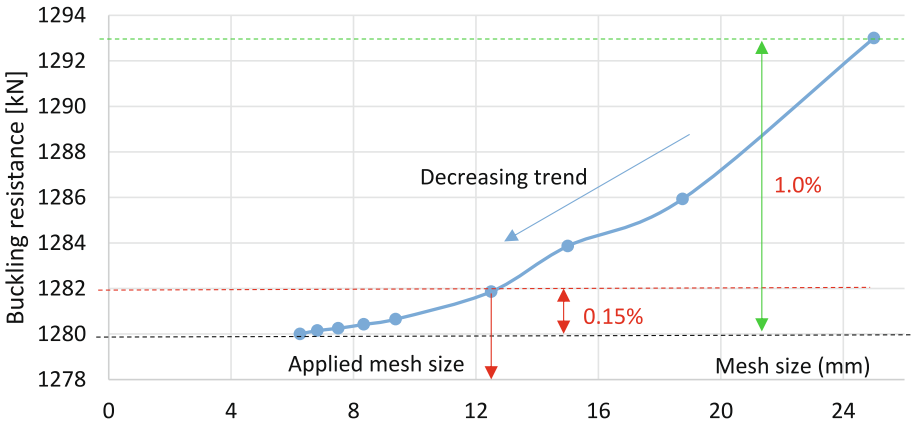

Fig. 2. Result of a mesh sensitivity analysis.

size that generated reliable results in a reasonable time is at least 8 elements in the transverse direction and 8*N_c in the longitudinal direction with an error of 0.15% from the smallest analysed mesh size. As shown in Fig. 2, the difference between the largest and the smallest mesh size was about 1%. Additionally, the results show that decreasing the mesh size results in a decrease in the ultimate load of the section. This proves the importance of the discretisation error check by applying a suitable mesh size to yield appropriate ultimate strength.

Imperfections exist in plates due to the fabrication and manufacturing processes. In numerical modelling, this can be achieved in different ways, for example, by using the first eigenmode of linear buckling analysis or by hand-defined imperfections. In the current study, local imperfection is modelled manually through modification of the perfect shape of the specimens. The shape of the local imperfection is a continuous half-sine waves consisting of three half-sine waves on each side along the longitudinal axis with amplitudes having opposite signs on the adjacent sides. The shape of the local imperfection is defined in both directions (longitudinal and transversal) according to *Eq. (8)* as shown in Fig. 1.

$$U^{F}_{L,Y} = U_{amp,loc}.sin\left(\frac{\pi\ .\ N_w.(i-1)}{N_c}\right) \tag{8}$$

Where $U_{amp,loc}$ is the amplitude of the imperfection (changed during the numerical parametric study), N_c is the number of plates defined along the cross-section, N_w is the number of half-sine waves along the length of the column (always 3 in the current study), i is the integer of the loop that goes from 1 to $N_c + 1$. The imperfections from *Eq. (8)* were added or subtracted to the proper coordinate of the nodes to introduce the imperfections at each node for each side of the column, depending on the sign of the imperfection and the location of the node. Separate imperfection sensitivity analysis has been performed to identify the most appropriate imperfection shape for the problem under investigation, which results are presented in Section 3.5.

3.2. Applied material models

In the current analysis, different material models are used for NSS and HSS materials. For the NSS, a quad-linear material model, as given by *Eqs. (9)-(14)* and presented in Fig. 3, is applied. This material model has been proposed by Gardner et al. to accurately capture the yield plateau and strain-hardening behaviour of structural carbon steels, based upon a large dataset of tensile coupon test results [19,20].

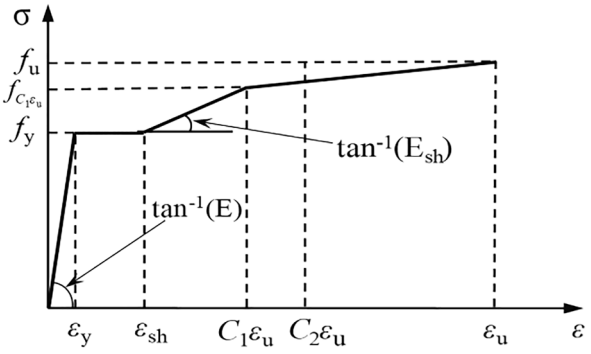

Fig. 3. The applied material model for NSS according to prEN 1993–1-14 [2].

$$\sigma(\varepsilon) = \begin{cases} E\varepsilon & ,\varepsilon \le \varepsilon_y \\ f_y & ,\varepsilon_y < \varepsilon \le \varepsilon_{sh} \\ f_y + E_{sh}(\varepsilon - \varepsilon_{sh}) & ,\varepsilon_{sh} < \varepsilon \le C_1\varepsilon_u \\ f_y C_1\varepsilon_u + \dfrac{f_u - f_y C_1\varepsilon_u}{(\varepsilon_u - C_1\varepsilon_u)}(\varepsilon - C_1\varepsilon_u) & ,C_1\varepsilon_u < \varepsilon \le \varepsilon_u \end{cases} \tag{9}$$

$$E_{sh} = \frac{f_u - f_y}{C_2\varepsilon_u - \varepsilon_{sh}} \tag{10}$$

$$\varepsilon_{sh} = 0.1\frac{f_y}{f_u} - 0.055,\ but\ 0.01 \le \varepsilon_{sh} \le 0.03 \tag{11}$$

$$\varepsilon_u = 0.6\left(1 - \frac{f_y}{f_u}\right),\ but\ 0.06 \le \varepsilon_u < A \tag{12}$$

$$C_1 = \frac{\varepsilon_{sh} + 0.25(\varepsilon_u - \varepsilon_{sh})}{\varepsilon_u} \tag{13}$$

$$C_2 = \frac{\varepsilon_{sh} + 0.4(\varepsilon_u - \varepsilon_{sh})}{\varepsilon_u} \tag{14}$$

Where $\varepsilon_y = f_y/E$ is the yield strain, ε_{sh} is the strain hardening strain, E_{sh} is the strain hardening modulus, A is the elongation after fracture defined in the relevant material specification (0.2 is used in the current analysis), C_1 coefficient defines a "cut-off" strain to avoid over-predictions of material strength, and C_2 is employed in *Eq. (10)* to determine the strain-hardening slope E_{sh}. The calculated parameters of this material model for the three studied steel grades are summarised in Table 1.

For HSS materials, the Ramberg-Osgood-type material model is

Table 1
The applied material model parameters.

	S235	S355	S460
f_y	235	355	460
f_u	360	510	540
ε_{sh}	0.010	0.015	0.030
ε_u	0.208	0.182	0.089
C_1	0.287	0.310	0.505
C_2	0.430	0.448	0.604
E_{sh}	1578	2310	3407
$C_1 \cdot \varepsilon_u$	0.060	0.057	0.045
$f_{C1\varepsilon u}$	313	451	510

applied in the numerical simulations, which is a non-linear elastic–-plastic material model using strain hardening. Usually, coupon tests are used to estimate the n parameter in the formula of the Ramberg-Osgood material model according to *Eqs. (15)-(16)*, in the current study, $n = 14$ is applied based on previous material tests available for the authors on the investigated steel materials [25]. The modulus of elasticity of 210,000 is assumed for all tests with Poisson's ratio of$\nu = 0.3$. Table 2 gives a summary of the material properties of the analysed steel grades, and Fig. 4 present the character of the applied material models.

$$\varepsilon = \frac{\sigma}{E} + 0.002 \cdot \left(\frac{\sigma}{f_y}\right)^n \tag{15}$$

Where n is equal to the log of the strains at any two points to the log of the stresses at any two points for the different coupon test, as shown in Eq. (16).

$$n = \frac{\log\left(\frac{\varepsilon_1}{\varepsilon_2}\right)}{\log\left(\frac{\sigma_1}{\sigma_2}\right)} \tag{16}$$

3.3. Applied residual stress model

Residual stress has a large influence on the buckling capacity of compression columns because it can cause premature yielding and loss of stiffness. The establishment of an accurate residual stress model is important in numerical simulations. Therefore, previous investigations on the local buckling and the residual stresses of welded box-section columns are studied in the international literature. There are many previous investigations dealing with the residual stress pattern of box-section columns [21–23], which are studied and compared in the current investigations. The typical distribution of residual stresses within welded cross-sections is shown in Fig. 5, which had common in all the previous investigations, where '+' represents tensile stress and '−' represents compressive stress. The value for the tensile (σ_t) and compressive residual stresses (σ_c) is taken according to Table 3 based on the recommendations of the prEN 1993–1-14 [2], which model is aligned with the ECCS recommendations (European Convention for Constructional Steelwork). Most of the analysed cross-sections in the current study are close to the H/t ratio of 40 or larger to investigate slender columns with local buckling type failure mode.

In the case of HSS members, the value for compressive residual stresses (σ_c) is taken equal to 0.13* 355 MPa for all the different steel grades, since different studies have shown HSS has lower compressive residual stresses compared to normal strength steel and the maximum values are independent of the steel grade [21–23]. The value for the tensile residual stress (σ_t) is always taken equal to the yield strength (f_y), and the width of the compression zone is calculated based on equilibrium equations. Therefore, the utilised values for the width of the tensile zone (a and b) are approximately equal to the values shown in the table below for light welding, ensuring equilibrium within the cross-section.

Table 2
Material properties for different types of steel.

Steel grade	Yield strength (f_y) (MPa)	Ultimate strength (f_u) (MPa)
S500	500	625
S690	690	850
S960	960	1115

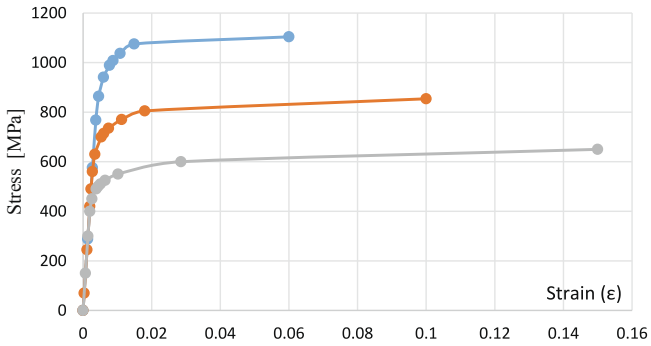

Fig. 4. The applied material model for HSS.

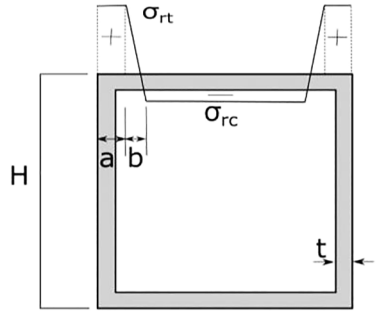

Fig. 5. Applied residual stress model for welded box-section columns.

Table 3
Parameter values for residual stress model according to [2].

H/t	Welding type	σ_{rt}/f_y	σ_{rc}/f_y	a	b
10	–	1.0	−0.60	0	–
20	Heavy weld	1.0	−0.82	3 t	3 t
20	Light weld	1.0	−0.29	1.5 t	1.5 t
40	Heavy weld	1.0	−0.29	3 t	3 t
40	Light weld	1.0	−0.13	1.5 t	1.5 t

3.4. Validation of the numerical model

Model verification is executed to show that the developed numerical model is accurate and can be used through the numerical parametric study to predict the ultimate load and buckling behaviour of the analysed stub columns. Validation of the numerical model is performed via a comparison of the computed resistance to test results available in the international literature. In the validation process, always measured material properties are applied. The samples were taken from three different research programs: (i) five specimens are taken from Bridge's research work [13], (ii) the second set consists of three samples from Clarin's research program [8], and (iii) the remaining samples were taken from Schillo's research work [15]. The first set contains S235 steel grade with plate slenderness ranging from 0.68 to 2.12. The second set contains a steel grade of S420 with different geometrical properties representing the range of plate slenderness within the range of 0.75 to 1.39. The third set consists of different steel types, including S500, S700, and S960, for a range of slenderness of 0.75 to 1.39. The details of each

test are shown in Table 4, including the steel grade, the local buckling slenderness $\bar{\lambda}_p$, section width b, height h, thickness t, length L, yield strength f_y, ultimate strength f_u, the ultimate force of the experiment $F_{u,\exp}$, the ultimate force of the numerical test $F_{u,num}$. Numerical tests were performed using the previously introduced numerical model, utilising the mentioned material models and a b/200 local imperfection. The comparison of the load–displacement diagrams is presented in Fig. 6 for two cases, but similar comparisons are made for all studied test specimens. The first test (left) is taken from Shillo's research program [15], the second test (right) is taken from Clarin's research program [8]. The obtained ultimate loads are close to the test results, which proves the applicability and accuracy of the numerical model. Fig. 7 shows the total deformation, and von Mises stresses of the first sample from Clarin's research program, shown in Table 4 with $b = 101.3$ mm and $\bar{\lambda}_p = 0.83$.

The results in Table 4 show the numerical model gives the closest values in the case of Schillo's research program. This research program is the most recent within this research topic, and it is detailed and accurately documented, so the numerical model results can be considered the most reliable for these specimens. It should also be mentioned that for some cases, the numerical model using b/200 imperfection predicted smaller or larger buckling resistance than measured in the laboratory, highlighting that the imperfection applied in the numerical model is not always perfect. It needs revision. It has also been observed that in the smaller slenderness range, the numerical model is typically underpredicted, while in the large slenderness range typically overpredicted the test results.

3.5. Analysis of imperfection shape on buckling resistance

This section discusses the effect of column length, the number of half-sine waves, the sign of the imperfection and the applied local buckling shape and presents the best imperfection configuration to achieve the lowest local buckling resistance of slender columns. Two smaller parametric studies are performed to study the effect of column length and the number of applied half-sine waves on the buckling resistance and modelling method of box-section columns. In the first parametric study, both the column length and the number of half-sine waves were changed, while in the second parametric study, only the number of half-sine waves was changed with a fixed column length. All parametric studies in this section were made on S355 with a constant imperfection magnitude of b/200.

The sensitivity analysis is performed by changing the number of half-sine waves as well as the length of the columns from the length of 1xb with one half-sine wave to the length of 4xb with four half-sine waves, where b is the width of the cross-section. As it can be seen in Fig. 8, the maximum difference in the ultimate force between one half sine wave and four half sine waves is less than 2%, but the significant difference occurs between the wave numbers of 1 and 3. The reason for it is that in the case of using one half-sine wave, the modelling method of the end supports could have a slight influence on the results. However, in the case of at least three buckling waves, this effect becomes negligible. Therefore, within the further parametric study to be performed, the selected length was always equal to $L = 3xb$.

To study the effect of the number of half-sine waves, an analysis is executed to determine the buckling resistance of a column having a length equal to $L = 3xb$ and changing the number of half-sine waves. Fig. 9 shows the computed buckling resistances using a different number of half-sine waves changing from one to eleven. Results prove three half-sine waves yields the lowest resistance in the case of specimen length equal to three times the width of the plate. Therefore, this configuration is used in further studies.

A concise parametric analysis study is also performed to investigate the effect of the applied buckling shape for the same local imperfection of *b/200* on four different column sections with lengths equal to three times the width, as discussed previously. In this case, eigenmode shapes are applied as imperfections. A total of ten local buckling shapes were generated for each section, and the numerical simulations are executed using the different eigenmode type imperfections. Results are shown in Fig. 10, showing that the first mode shape yields the lowest resistance, and all the other modes lead to higher resistances. Therefore, the first buckling shape that consists of three alternating half-sine waves would be utilised in the investigations. It should also be mentioned that the buckling resistance difference using the hand defined three half-sine wave or the first eigenmode shape method is negligible in the case of the analysed specimens.

The effect of the sign of the imperfection is also analysed by performing two different tests with different signs of imperfection and having the same imperfection amplitude, as shown in Fig. 11. Both columns showed the same buckling resistance and the deformation values, and the obtained differences are negligible (smaller than the numerical tolerance of the applied solver).

Based on the applied imperfection sensitivity analyses, it is concluded that three half-sine waves with a length of three times the width of the plate, or applying the first eigenmode shape having local buckling, would generate the lowest resistance. Therefore, the following parametric study investigates this configuration.

4. Results of the numerical parametric study

4.1. Parameters used in the numerical parametric study

The numerical parametric study aims to find the suitable imperfec-

Table 4
Results of the model validation.

Steel grade	λ_p	b (mm)	h (mm)	t (mm)	L (mm)	f_y (MPa)	f_u (MPa)	$F_{u,exp}$ (kN)	$F_{u,num}$ (kN)	$\frac{F_{u,num}}{F_{u,exp}}$
S235	0.68	80	80	2.14	280	282	324	182.1	183.8	1.00
S235	1.06	121.5	121.5	2.14	418	282	324	183.8	216.3	1.17
S235	1.41	160.9	160.9	2.14	554	282	324	184.2	226.6	1.23
S235	1.77	200.3	200.3	2.14	690	282	324	210.9	241.1	1.14
S235	2.12	240	240	2.14	832	282	324	222.2	254.2	1.14
S420	0.75	101.3	101.3	3.05	326	441	529	505.9	493.36	0.97
S420	0.89	119.4	119.4	3.05	380	441	529	468.4	537.20	1.14
S420	1.39	181.3	181.3	3.05	571	441	529	502.4	574.86	1.14
S500	0.83	195	195	6.0	650	562	618	2261	2280.00	1.01
S700	0.90	181	181	6.0	588	760	822	2716	2552.90	0.94
S700	1.32	260	263	6.0	828	760	822	2667	2663.57	0.99
S960	0.65	120	121	6.0	410	992	1024	2932	2783.88	0.95
S960	0.94	170	170	6.1	560	992	1024	3362	3071.25	0.91
S960	1.24	219	222	6.1	710	992	1024	3196	3212.99	1.00

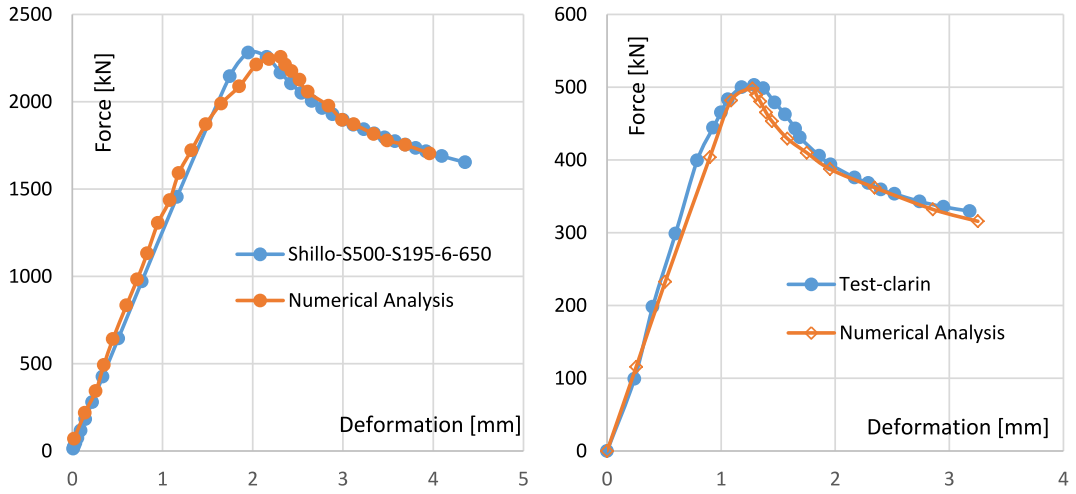

Fig. 6. Comparison of measured and computed load-deformation curves. a) for Schillo's test specimens B260-6–2000 [15] and b) Clarin's test specimen S20-0a [8].

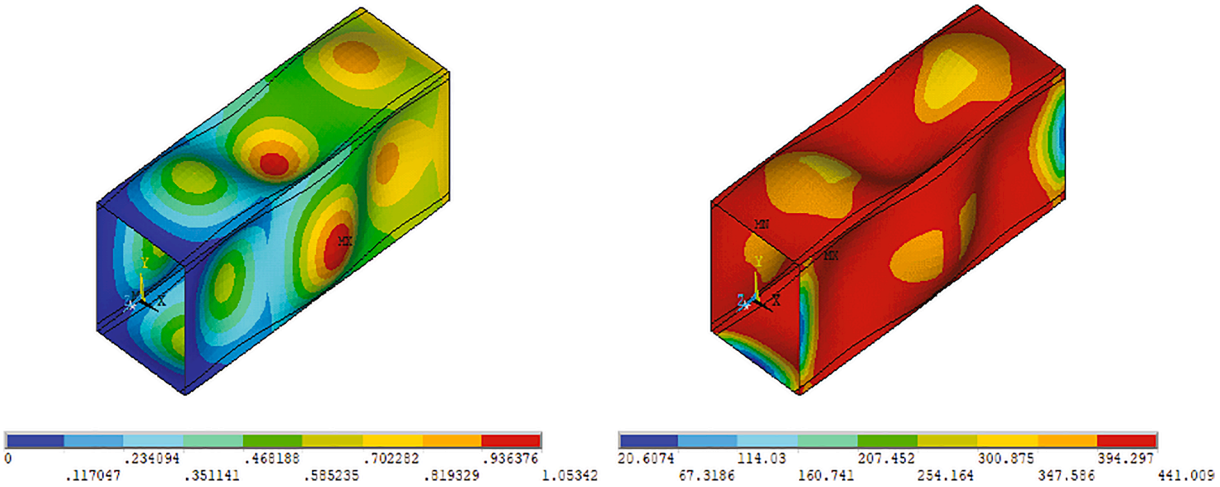

Fig. 7. Obtained failure mode for local buckling at the final step of loading of the first Clarin's test specimen; a) deformed shape [mm], b) von Mises stresses [MPa].

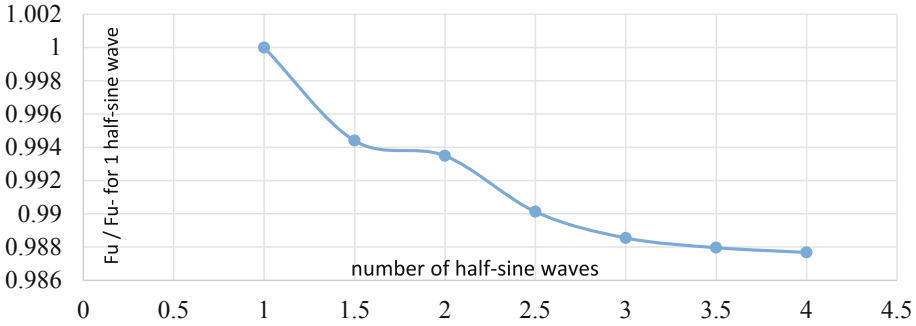

Fig. 8. Buckling resistance depending on specimen length and number of half-sine waves.

tion factors and their combination with residual stresses for the normal and high strength steel box-section columns. The analysed cross-sections had b/t ratio larger than 40 and a local slenderness ratio ($\bar{\lambda}_p$) larger than 0.7. Only square box sections are investigated within the current parametric study covering a wide range of width-to-thickness ratios and cross-section dimensions. The relative slenderness ratio is changed between 0.7 and 2.8 in the parametric study. The width of the analysed panel is varied between 200 mm and 450 mm. The thickness of the plates is changed between 2.5 and 12 mm with 0.5 mm increment resulting in different slenderness ratios. The parametric study and the result evaluation are divided into two parts, the first part is concerned with NSS (S235, S355, and S460) material, and the second part contains HSS (S500, S700, and S960) materials, so a total of six different steel grades are covered in the current study. The applied geometries, a combination of b = h and t values, are given in Table 5.

Each geometry is studied twice: (i) with equivalent geometric imperfections and (ii) with geometric imperfections and residual stresses. For each analysed cross-section geometry, imperfection sensitivity

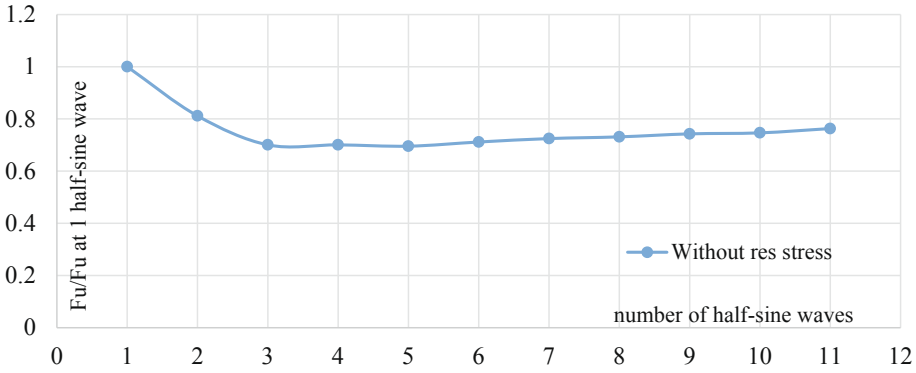

Fig. 9. Sensitivity of the column for the number of the implemented half-sine waves for a fixed length of 3.b.

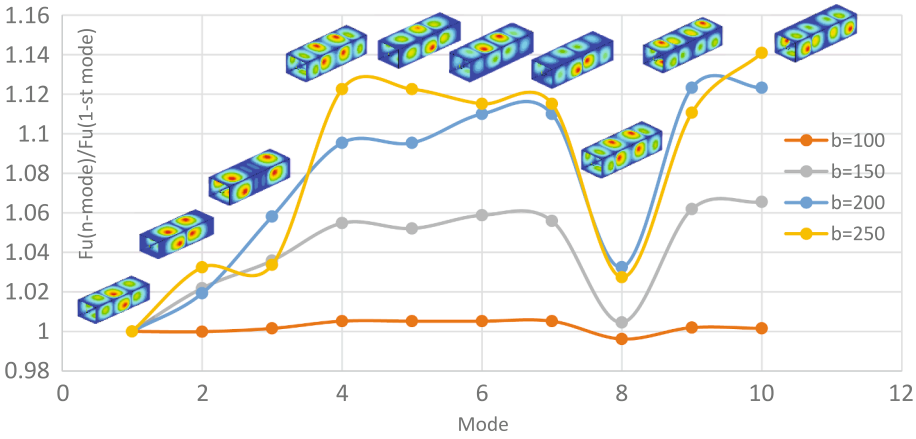

Fig. 10. Relative buckling resistance using different eigenmode shapes as imperfections.

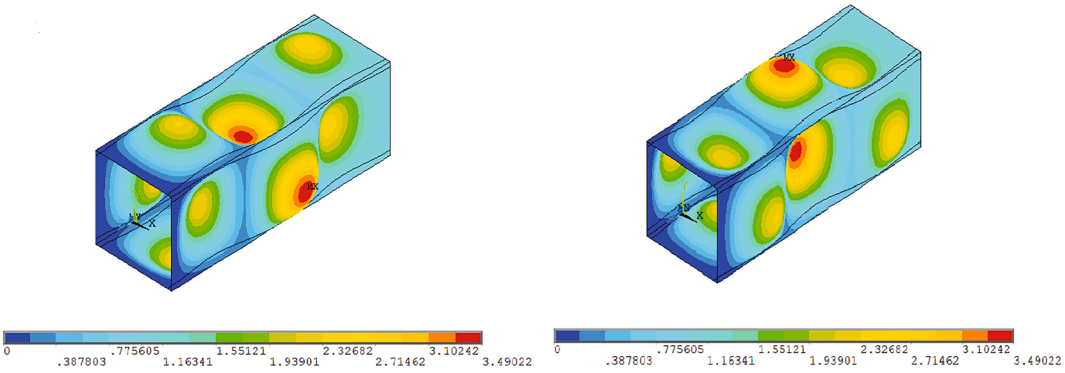

Fig. 11. Effect of imperfection direction on buckling shape.

analysis is executed, and the change in the buckling resistance with the imperfection magnitude is evaluated individually. More than 7000 GMNI analyses are performed in the current research program to determine the buckling resistance having different combinations of imperfections and residual stresses for both NSS and HSS structures.

4.2. Effect of imperfections on the ultimate force obtained during the analysis

Imperfection sensitivity analysis is executed for each analysed cross-section geometry. One example is presented in Fig. 12. The horizontal axis presents the applied imperfection scaling factor in the form introduced by *Eq. (17)*. The vertical axis presents the reduction factor for local buckling calculated by *Eq. (18)*, where F_{num} is the numerically calculated buckling resistance, A_c is the gross cross-sectional area, and f_y is the yield strength of the applied material.

$$Local\ imp.\ magnitude = \frac{width\ of\ the\ plate(b)}{imp.scaling\ factor(f)} \tag{17}$$

$$\rho_{num} = \frac{F_{num}}{A_c.f_y} \tag{18}$$

Within the imperfection sensitivity study reduction factor at each specific local imperfection is calculated according to *Eq. (18)* and plotted against its corresponding imperfection. As shown in the graph, by keeping all the parameters the same and changing only the

Table 5
Geometrical properties of the analysed cross-sections.

	b = h [mm]	thickness values [mm]
1	200	2.0; 2.5; 3.0; 3.5; 4.0; 4.5; 5.0; 5.5; 6.0; 6.5;
2	250	2.0; 2.25; 2.5; 2.75; 3.0; 3.25; 3.5; 4.0; 5.0; 6.0; 7.0; 8.0
3	300	2.75; 3.0; 3.5; 4.0; 4.25; 4.5; 4.75; 5.0; 5.25; 5.5; 5.75; 6.0; 6.5; 7.0; 8.0; 9.0
4	350	2.75; 3.0; 3.5; 4.0; 4.5; 5.0; 5.5; 6.0; 6.5; 7.0; 8.0; 9.0; 10.0
5	400	3.5; 3.75; 4.0; 4.25; 4.5, 4.75; 5.0; 5.5; 6.0; 6.5; 7.0; 8;0
6	450	3.75; 4.0; 4.25; 4.5; 4.75; 5.0; 5.25; 5.5; 5.75; 6.0; 6.5; 7.0; 8.0; 9.0; 10.0; 11;0

All geometries are investigated using steel grades of.
NSS: S235, S355, S460
HSS: S500; S700; S960

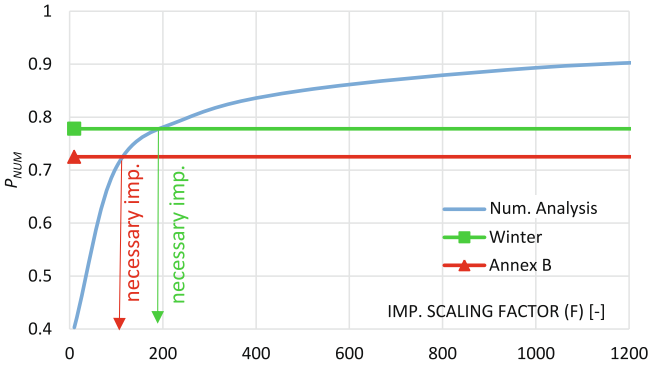

Fig. 12. Results of imperfection sensitivity analysis.

imperfection scaling factor (f) from 10 to 1200, the local buckling reduction factor ρ_{num} is changing significantly. The buckling reduction factors calculated by the Winter-type and Annex B curves are marked by horizontal lines on the graph. Taking the intersection points between both lines (acc. to Winter and Annex B curves) with the numerical calculation results the necessary imperfection magnitudes are determined. The obtained values indicate the points where the numerical model leads to exactly the same buckling resistance as predicted by the Winter-type or Annex-B curves. These points are shown by the vertical arrows in Fig. 12. It is visible on the results, to reproduce the Winter-type curve requires a larger imperfection than the Annex B curve.

The imperfection sensitivity analysis is executed for all analysed cross-sections and steel grades. One comparison is presented in Fig. 13, showing the differences in the imperfection sensitivity depending on the plate slenderness ratio ($\bar{\lambda}_p$). Results show at the range of plate slenderness between$\bar{\lambda}_p = 0.7$ to 1.3, the imperfection factor has a large impact on the reduction factor, while for smaller and larger slenderness ratios,

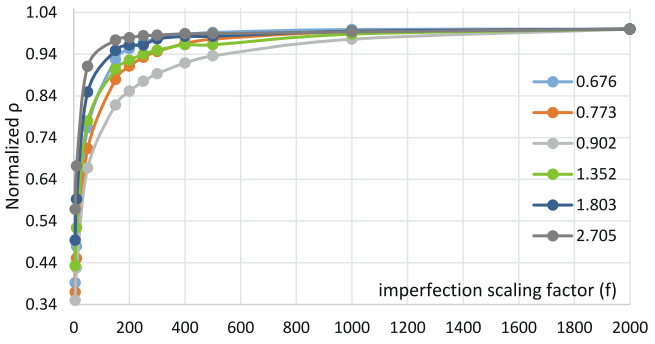

Fig. 13. Relationship between the imperfection scaling factor (f) and the normalised buckling reduction factor (ρ) for S355 steel grade using equivalent geometric imperfections.

the effect of the imperfection factor tends to decrease. The same phenomenon can be noticed in the presence of residual stresses, and it is more pronounced in this case, where the values of the normalised ρ tend to be equal to 1 at the very high slenderness range. It can be concluded, according to a large number of numerical results, the imperfection sensitivity is the largest for plates within the middle-range slenderness. For small and large slenderness ratios, the effect of imperfections is smaller.

4.3. Necessary imperfections for normal strength steel structures

4.3.1. Using equivalent geometric imperfections

The necessary equivalent geometric imperfection magnitudes are determined for all analysed cross-sections (as presented for one specific case in Fig. 12). All the obtained data points are shown in Fig. 14 for all the three analysed steel grades and to both buckling curves. On the horizontal axis, the relative slenderness ratio of the analysed cross-section is presented. The vertical axis represents the necessary imperfection scaling factor for equivalent geometric imperfections. Results are separately evaluated and presented regarding the Winter-type or Annex B buckling curves. Results show that the necessary imperfection strongly depends on the relative slenderness ratio of the plate and cannot be given with one specific constant value, always resulting in a safe side resistance as currently given in the EN 1993–1-5 [1] or prEN 1993–1-14 [2]. Results prove the standardised imperfection $b/200$ leads to smaller resistance than predicted by the Winter-type curve for slenderness ratios of$\bar{\lambda}_p \leq 1.8$. In the case of a larger slenderness ratio, the numerical model results in larger resistances than predicted by the Winter-type curve leading to unsafe side resistance. In the case of the Annex B curve, the required imperfection magnitude would be significantly larger within the entire analysed slenderness range than the standardised value of $b/200$. Results also show that the yield strength has a significant effect on the necessary imperfection scaling factor. Increasing the yield strength results in an increased reduction factor (which is independent of the yield strength). Therefore, larger imperfections are to be applied, resulting in the same buckling resistance as predicted by the Winter-type curve or the Annex B curve. It is worth mentioning that curves tend to coincide at the very large plate slenderness $\bar{\lambda}_p$. This happens because both the Winter-type and Annex B curves are flattening at a high slenderness ratio $\bar{\lambda}_p$, and the imperfection sensitivity of the analysed cross-sections tends to become smaller.

Fig. 14 shows the necessary equivalent geometric imperfection factor that follows a clear trend depending on the relative slenderness ratio, which can be mathematically described. Lower bound curves to the numerical data points are also presented in Fig. 14 separately to each steel grade and buckling curve. *Eqs. (19)-(21)* gives the mathematical formulations of the presented lower bound trend lines, where the yield strength should be given in [MPa]. A fixed plateau (constant value) was chosen to represent the concaved part of the curve to achieve safe side and reasonable results with simplified equations and fitting procedures. As it can be seen, equations are relatively simple to calculate and provide a convenient estimation of imperfection scaling factors (f) in the design practice.

Design proposal to Winter-type curve:

$$f_{Winter} = \frac{3525 - 3.12 \cdot f_y}{8.35}, \ \ if \ \bar{\lambda}_p \leq 1.7 \tag{19}$$

$$f_{Winter} = \frac{1}{\bar{\lambda}_p^{\,4}} \cdot \left(3525 - 3.12 \cdot f_y\right), \ \ if \ \bar{\lambda}_p > 1.7 \tag{20}$$

Design proposal to Annex B curve:

$$f_{Annex\_B} = \frac{1}{\bar{\lambda}_p^{\,2.2}} \cdot \left(200 - 0.2 \cdot f_y\right) \tag{21}$$

To check the accuracy of the proposed equations a statistical analysis

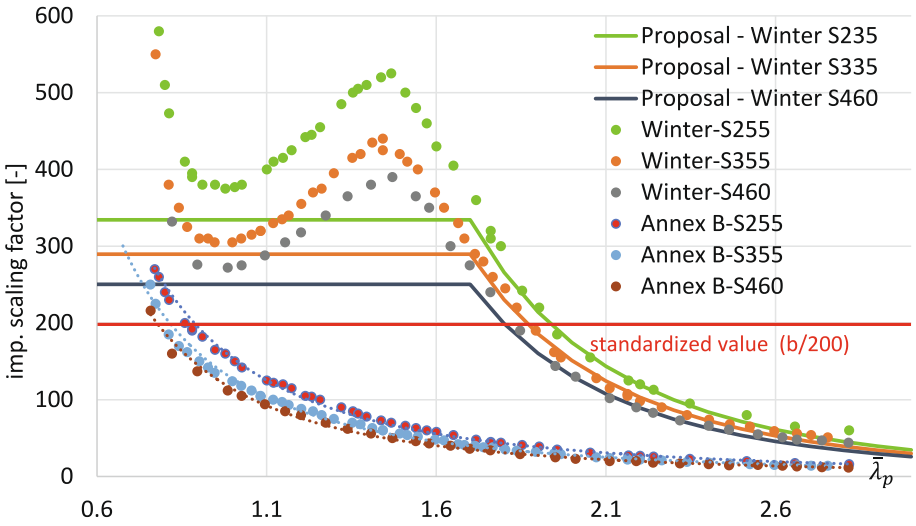

Fig. 14. Relationship between the plate slenderness $\bar{\lambda}_p$ and the imperfection scaling factor (f) for different steel grades and proposed design curves.

is executed using JASP statistical software, the obtained results are summarised in Tables 6-7 for the two buckling curves separately. To perform this statistical analysis, GMNIA analyses are executed for each cross-section geometries again using the imperfection magnitude proposed by the given equations. Then, the computed buckling resistance is compared to the buckling resistance determined by the Winter-type curve or Annex B curve, respectively. The statistical evaluation is executed on this new database to check the accuracy of the given equations regarding the buckling resistance. The variable in the statistical analysis is the ratio of buckling resistance of the numerical test divided by the buckling resistance of Annex B curve or Winter-type curve, and all the statistical measures, shown in the following tables, are applied to it.

It can be seen by the different statistical measures the proposed magnitude to the equivalent geometric imperfection results in a good estimation of the buckling resistance compared to the standardised buckling curve while the mean value is extremely close to 1.0 and results have a relatively small standard deviation.

4.4. *Using geometric imperfections and residual stresses*

A similar parametric study, as presented in the previous section, has been conducted on the numerical model just using geometric imperfections and residual stresses. In the current study, the residual stresses introduced in Table 3 are applied, assuming that light welding is used. Imperfection sensitivity analysis has also been executed, changing the magnitude of the geometric imperfection, but the residual stress pattern and the maximum values of the residual stresses are not changed. The reason for that is that the magnitude of the geometric imperfections is to be determined, leading to the same buckling resistance as provided by the Annex B curve using the predefined residual stress model. Based on the imperfection sensitivity study, the buckling resistance and the necessary imperfection scaling factors are determined for all analysed cross-sections, and the obtained values are evaluated depending on the relative slenderness ratio, as presented in Fig. 15. Results prove the trend of the necessary imperfection factor is similar to the trend presented in the previous section in the case of the equivalent geometric imperfections; However, the values are significantly different. It was anticipated that smaller imperfection factors are needed in the presence of residual stresses compared to their absence. It can also be observed, the difference between the obtained results depending on the steel grade is significantly smaller than for the equivalent geometric imperfections, especially at the high slenderness range ($\bar{\lambda}_p > 1.4$) as shown in Fig. 15.

Table 6
Statistical measures of the numerical results for S235, S355, and S460 steel grades compared to the Annex B curve.

Statistical measure/curve	Annex B - S235	Annex B - S355	Annex B - S460
Number of tests	45	51	31
Mean	1.002	1.004	0.996
Median	0.999	0.999	0.996
Standard deviation	0.012	0.019	0.012
Skewness	0.043	0.189	1.049
Kurtosis	−0.822	1.570	1.348
Minimum value	0.978	0.942	0.979
Maximum value	1.022	1.050	1.029

Table 7
Statistical measures of the numerical results for S235, S355, and S460 steel grades compared to the Winter-type curve.

Statistical measure/curve	Winter-type curve - S235	Winter-type curve - S355	Winter-type curve - S460
Number of tests	45	55	31
Mean	1.003	1.003	1.001
Median	1.001	1.002	1.001
Standard deviation	0.013	0.014	0.012
Skewness	−0.191	−0.334	−0.011
Kurtosis	−0.350	0.661	0.139
Minimum value	0.970	0.960	0.971
Maximum value	1.028	1.029	1.024

The mathematical formulation for the proposed curves, yielding to the buckling resistance according to Annex B curve, is given by *Eq. (22)*.

Mean curve:

$$f_{NSS} = \begin{cases} 675 - 0.53 f_y, \bar{\lambda}_p < 1.2 \\ \left(2.65 f_y - 3010.5\right)\bar{\lambda}_p + \left(-3.71 f_y + 4287.6\right), 1.2 \le \bar{\lambda}_p < 1.4 \\ \dfrac{200}{\bar{\lambda}_p^{\,3}}, \bar{\lambda}_p \ge 1.4 \end{cases} \tag{22}$$

To check the accuracy of the proposed equation, statistical analysis is also executed on the database using the computed buckling resistances obtained by the imperfection scaling factor provided by *Eq. (22)*. Results of the statistical analysis are given in Table 8, showing the proposed equation gives a good estimation of the magnitude of the geometric imperfections using the residual stress pattern introduced in Section 3.3. The application of the geometric imperfections and residual stresses has

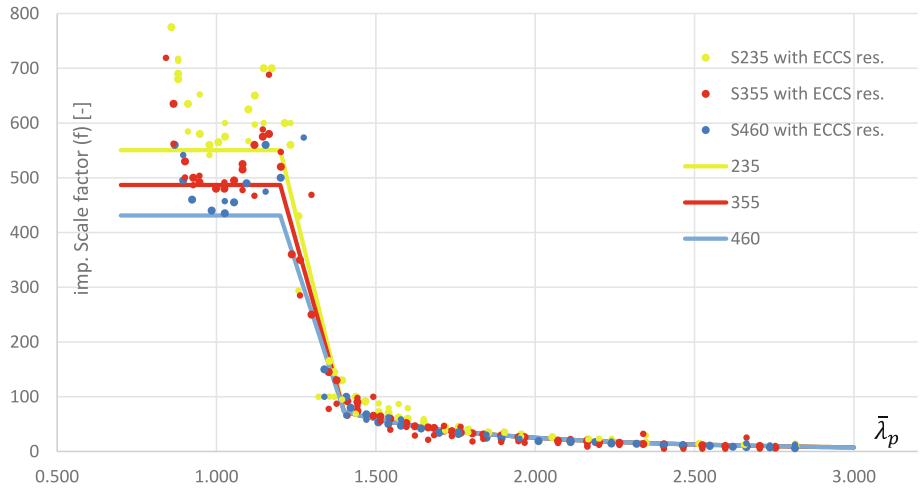

Fig. 15. Relationship between the plate slenderness ratio $\bar{\lambda}_p$ and the imperfection scaling factor (f) for S235, S353, and S460 steel grades with residual stresses.

Table 8
Statistical measures of the numerical results for S235, S355, and S460 steel grades compared to the Annex B curve.

Statistical measure/Curve	S235	S355	S460
Number of tests	45	55	31
Mean	0.975	0.987	1.002
Median	0.973	0.984	1.001
Standard deviation	0.017	0.024	0.031
Skewness	−0.308	−0.537	−0.231
Kurtosis	0.176	1.585	0.157
Minimum value	0.930	0.915	0.992
Maximum value	1.009	1.037	1.060

importance in the case of structures, where many different stability problems are to be introduced, and the effect of the residual stresses are not intended to be applied many times, resulting in conservative results. The importance is this phenomenon for the interaction of global and local buckling resistance is shown by Degée et al. [24] in 2008.

Results presented in Fig. 15 also indicates that relatively large geometric imperfection should be applied with residual stresses to achieve the buckling resistance presented by the Annex B curve, which is not in line with the manufacturing tolerances. The manufacturing tolerance for this cross-section type (out-of-plane imperfections of plate panels between webs or stiffeners, general case) is equal to $\Delta = \pm b/125$ according to EN 1090–2:2018 Table B.4 No. 3 [26]. It means that the buckling resistance for cross-sections having larger slenderness than 1.3 could be underestimated by the imperfection magnitudes given by *Eq. (22)* referring to Annex B curve. Therefore, to demonstrate the difference, all the analysed geometries are recalculated having imperfection magnitudes given according to *Eq. (22)* but having a minimum imperfection scale factor of $f_{min} = 125$ fitting to the manufacturing tolerance.

Results in Fig. 16 show the computed reduction factors using imperfection given by *Eq. (22)* perfectly fits the Annex B buckling curve, however, results considering the allowed maximum manufacturing tolerances yields to reduction factors closer (slightly higher) to the buckling curve developed by Schillo [15]. These calculation results prove the applicability and accuracy of the buckling curve of Schillo for slender cross-sections, which had been experimentally and statistically evaluated and proved to be reliable, but according to the authors' knowledge, it has not been analysed until now by reliable numerical simulations. This observation also means the realistic buckling resistance of the analysed cross-sections in the large slenderness domain should be closer to the buckling curve proposed by Schillo. Therefore, the equivalent geometric imperfections to reach reliable buckling resistance needs revision, and *Eq. (21)* developed for the Annex B curve can be improved. The entire parametric study introduced previously in Section 4.3 has been recalculated, and the necessary imperfection scaling factors fitting to the buckling resistance according to Schillo are

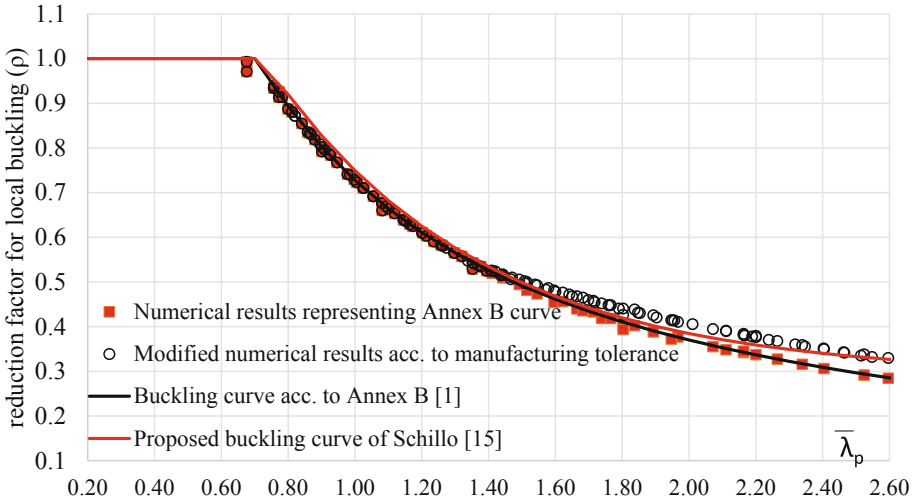

Fig. 16. Numerically calculated buckling reduction factors considering manufacturing tolerances for NSS structures.

determined. The best-fit approximation is given by *Eq. (23)*.

$$f_{Schillo} = \frac{1}{\bar{\lambda}_p^{2.2}} \cdot (200 - 0.2 \cdot f_y), \ \ if \ \bar{\lambda}_p \leq 1.35$$
$$f_{Schillo} = \frac{1}{\bar{\lambda}_p} \cdot (160 - 0.2 \cdot f_y), \ \ if \ \bar{\lambda}_p > 1.35 \quad (23)$$

4.5. Necessary imperfections for high strength steel structures

4.5.1. Using equivalent geometric imperfections

The same procedure is repeated by applying HSS materials. Fig. 17 shows the obtained necessary imperfection scaling factor to the equivalent geometric imperfection fitted to the Winter-type curve. The trend and the character of the results are similar to those presented for NSS. As steel types with higher yield strength need smaller imperfection scaling factors compared to the materials with lower yield strength. This is due to the nature of the Winter-type curve, there is no direct relationship between the Winter formula and the yield strength, only the plate slenderness $\bar{\lambda}_p$ depends on the yield strength. Therefore, high-strength steel structures require larger imperfection magnitudes to intersect with the results of the Winter-type buckling curve. Results show the curves tend to coincide with each other at the very large slenderness range ($\bar{\lambda}_p$ greater than 2.5). This happens due to the fact that for very large slenderness ratios, the structures have smaller imperfection sensitivity.

For the three different steel grades, three different curves are fitted to give a good estimation of the imperfection factors to be implemented in the numerical model. It can be noticed that a horizontal plateau was chosen to replace the region having large fluctuation in the slenderness range of ($\bar{\lambda}_p = 0.75 to 2.05$) and to ensure easy-to-apply imperfection value for the design practice. The choice of the plateau was done based on the minimum imperfection scaling factor (f), generating the largest imperfection value to get safe side results. The other part of each curve was chosen based on best fit with power equations in the form of $f = a.\bar{\lambda}_p^{b} + c$, where a, b, and c are constants depending on the steel type. The formulas representing the imperfection scaling factor (f) for the different steel grades are given by *Eqs. (24)-(25)*.

$$f_{winter_{HSS}} = min(1300 - 0.95 \cdot f_y; a \cdot \bar{\lambda}_p^{b} + c) \quad (24)$$

$$a = -43.23 \cdot f_y + 3.1 \times 10^5$$
$$b = -0.0044 \cdot f_y - 5.76 \quad (25)$$
$$c = 0.023 \cdot f_y - 2.41$$

The results of the statistical evaluation are summarised in Table 9.

Table 9
Statistical measures of the numerical results for S500, S700, and S960 steel grades compared to the Winter-type curve.

Statistical measure/curve	Winter-S500	Winter-S700	Winter-S960
Number of tests	55	55	60
Mean	1.002	1.005	1.009
Standard deviation	0.022	0.019	0.018
Minimum value	0.971	0.961	0.976
Maximum value	1.040	1.042	1.048

For all the three different curves, the mean value is close to 1 with a relatively small standard deviation proving the accuracy of the proposed equation. Also, the minimum and maximum values are lying within the 5% range.

A similar procedure is carried out to estimate the imperfection factors that are needed to be implemented in the numerical model to generate ultimate resistance equal to calculated by the Annex B curve. The results are summarised in Fig. 18. Results show smoother curves are obtained, having a relatively small scatter. Trend lines are fitted to the database separately for all the three analysed steel grades, as shown on the graph. Equations describing these curves are given by *Eqs. (26)-(28)* depending on the yield strength and the relative slenderness ratio of the analysed cross-section. The statistical measure of the fitted curve and the buckling resistance according to Annex B is given in Table 10.

$$f_{Anxb_{HSS}} = a \cdot \bar{\lambda}_p^{-b} \quad (26)$$

$$a = -0.19 \cdot f_y + 276.6 \quad (27)$$

$$b = 9.9 \times 10^{-4} \cdot f_y - 3.45 \quad (28)$$

4.6. Using geometric imperfections and residual stresses

The same imperfection sensitivity analysis is executed for HSS materials considering residual stresses according to Section 3.3 and geometric imperfections. All the results are compared to the Annex B curve, and the magnitude of the necessary geometric imperfection is determined. The obtained results based on the numerical parametric study made on 165 analysed cases covering three steel grades and a wide range of slenderness ratios are presented in Fig. 19. The plot contains the mean and lower bound curves fitted to the numerical results. The obtained trend lines can be described by *Eqs. (29)-(30)*. Results also show that smaller imperfection scaling factors are needed for higher steel grades than for lower steel grades. It has a similar reason as described before. The related statistical measures are summarised in Table 11.

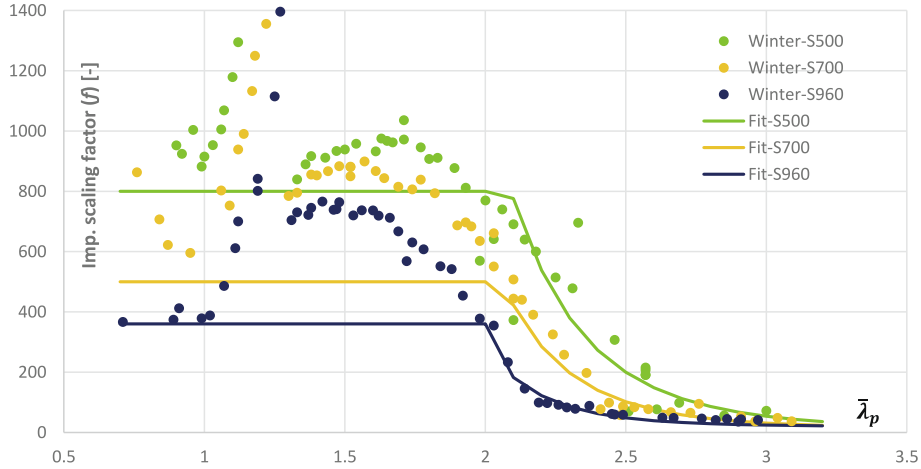

Fig. 17. Relationship between $\bar{\lambda}_p$ and imperfection scaling factor (f), for steel grades of S500, S700, S960 modelled without residual stresses and calibrated to Winter-type curve.

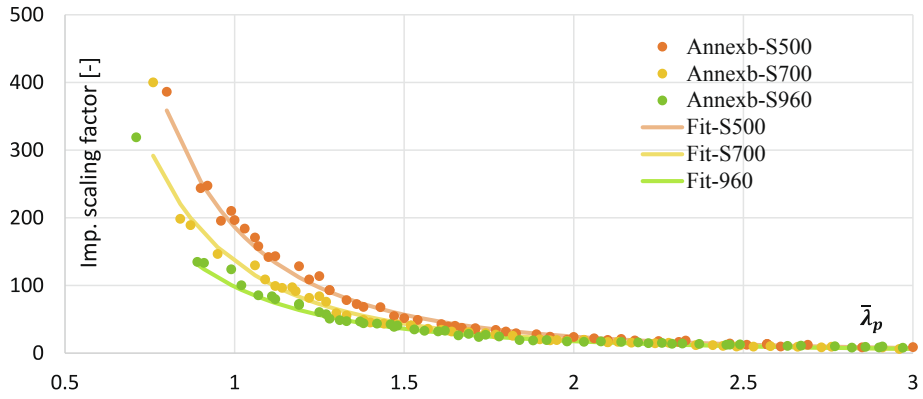

Fig. 18. Relationship between $\bar{\lambda}_p$ and imperfection scaling factor (f), for S500, S700, and S960 steel grades using equivalent geometric imperfections and calibrated against Annex b curve without residual stress.

Table 10
Statistical measures of the numerical results for S500, S700, and S960 steel-grades compared to the Annex B curve.

Statistical measure/curve	Annexb-S500	Annexb -S700	Annexb -S960
Number of tests	55	55	55
Mean	1.000	1.003	1.017
Standard deviation	0.013	0.951	0.015
Minimum value	0.965	3.799	0.565
Maximum value	1.023	1.029	1.049

$$f_{mean} = \begin{cases} 424 & ,\bar{\lambda}_p \le 1 \\ 420.\bar{\lambda}_p^{-5.5} & +4, \bar{\lambda}_p > 1 \end{cases} \quad (29)$$

$$f_{lowerbound} = \begin{cases} 330 & ,\bar{\lambda}_p \le 0.95 \\ 246.\bar{\lambda}_p^{-5.5} & +3, \bar{\lambda}_p > 0.95 \end{cases} \quad (30)$$

The total number of analysed cases was 165. Results prove the mean curve represents a good estimation for the buckling resistance with a relatively small standard deviation of 0.032 and with a small scatter represented by the minimum and maximum values of 0.947 and 1.101. For the lower bound curve, it can be concluded that this curve is a conservative estimation with a mean value around 0.95 and a standard deviation of 0.036. By utilising this curve in the analysis, the majority of the results would be on the safe side.

Results presented in Fig. 19 also indicates that relatively large geometric imperfection should be applied with residual stresses to achieve the buckling resistance presented by Annex B curve conflicting with the manufacturing tolerances. Therefore, all the analysed geometries are recalculated, applying residual stresses and geometric imperfections according to *Eq. (29)* but considering the manufacturing tolerance (f_{min} = 125). Fig. 20 shows the calculated results. It can be seen, the difference between the buckling resistances are significant for plates having larger local slenderness than 1.3 and all the buckling resistances calculated considering the manufacturing tolerance are located above the buckling curve proposed by Schillo. It means the proposed buckling curve is applicable for NSS and HSS structures and provides safe side buckling resistances in the analysed parameter range.

The equivalent geometric imperfections are also revised and *Eqs. (31)-(32)* developed for the Annex B curve are improved. The necessary equivalent geometric imperfections are reassessed, and the necessary imperfection scaling factors fitting to the buckling resistance according to Schillo are determined. The best-fit approximation is given by *Eq. (31)-(32)*.

$$f_{Schillo_{HSS}} = a \cdot \bar{\lambda}_p^{-3.65} \quad (31)$$

$$a = -0.3 \cdot f_y + 400 \quad (32)$$

Table 11
Statistical measures of the numerical results for S500, S700, and S960 steel-grades using residual stresses compared to the Annex B curve.

Statistical measure/curve	Mean	Lower bound
Number of tests	165	165
Mean	0.990	0.947
Standard deviation	0.024	0.078
Minimum value	0.941	0.864
Maximum value	1.053	1.040

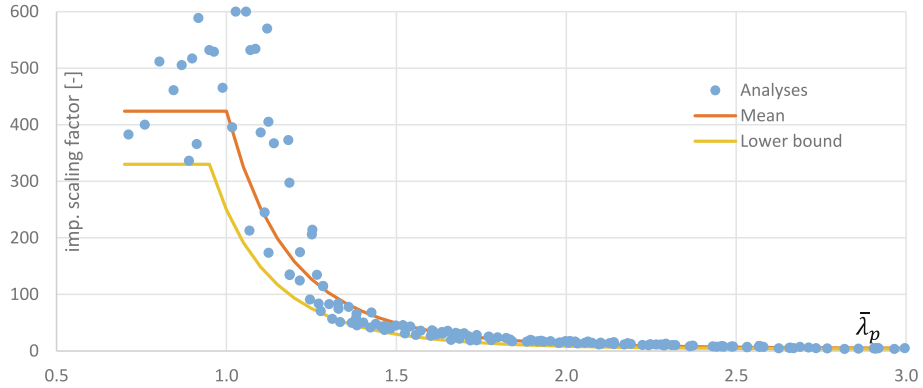

Fig. 19. Relationship between $\bar{\lambda}_p$ and imperfection scaling factor (f) for S500, S700, and S960 steel grades using residual stresses and geometric imperfections and calibrated against Annex B curve.

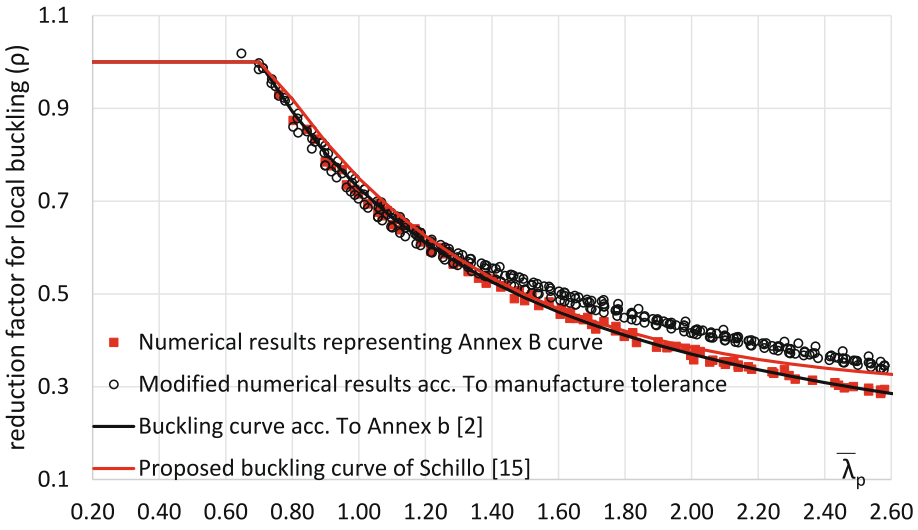

Fig. 20. Numerically calculated buckling reduction factors considering manufacturing tolerances for HSS structures.

5. Conclusions

The buckling curve provided by EN 1993–1-5 has been criticised by many researchers in the past and it has been proven that the buckling resistance provided by the Winter-type buckling curve does not always lead to safe side resistance and needs revision. Previous studies also proved the Annex B curve of the EN 1993–1-5 could lead to safe side resistances also for slender welded box-section columns subjected to pure compression. Therefore, the buckling curve to be applied has been changed. If the buckling curve changes, the equivalent geometric imperfection to be applied in FEM based design process should also be changed, which calibration process was completely missing from the international literature until now. Therefore, the main aim of the current research program is to find appropriate equivalent geometric imperfections and combinations of residual stresses and geometric imperfections to be used in a numerical model, obtaining an ultimate buckling resistance equal to the result provided by the Annex B curve or the buckling curve proposed by Schillo.

Within the current investigations, design equations are proposed to determine the equivalent geometric imperfections to be applied in the numerical model to accurately capture the buckling resistance of welded box-section columns for steel grades between S235 – S960. The current investigations proved that the imperfection scaling factor to be applied depends on the steel grade and the relative slenderness ratio of the analysed cross-section. The developed design equations consider these two parameters, and by the application of this imperfection scaling factor, the computed buckling resistance would fit the analytically determined bucking resistance provided by the Annex B or Winter-type curves or the buckling curve of Schillo. In the current analysis, hand defined half-sine wave shapes are used as imperfections, but the numerical analysis also proved the given imperfection magnitudes are also applicable by using the first eigenmode shape as imperfections.

Previous studies also proved the effect of residual stresses in the equivalent geometric imperfections and the buckling resistance has high importance if the interacting stability phenomenon is studied by the numerical model. There was a lack of previous investigations on the determination of the necessary geometric imperfections if residual stress models are also applied in the numerical analysis. Therefore, within the current research program, the necessary geometric imperfection scaling factors are determined. Design equations are developed to determine the magnitude of the necessary geometric imperfection for slender welded box-section columns having steel grades of S235 – S960. The proposed geometric imperfections, together with the applied residual stress model (residual stress pattern proposed by the ECCS), results in a good approximation to the buckling resistance provided by the Annex B curve of the EN 1993–1-5. Results also prove that if manufacturing tolerances are also considered in the geometric imperfections, buckling reductions factors close to the buckling curve proposed by Schillo would be achieved, which proves the accuracy and applicability of that buckling curve.

Declaration of Competing Interest

The authors declare that they have no known competing financial interests or personal relationships that could have appeared to influence the work reported in this paper.

Acknowledgement

The presented research program has been financially supported by the Grant MTA-BME Lendület LP2021-06 / 2021 “Theory of new generation steel bridges” program of the Hungarian Academy of Sciences and Stipendium Hungaricum Scholarship. Both grants are gratefully acknowledged.

References

[1] EN 1993-1-5: 2006 Eurocode 3-Design of steel structures. Part 1.5: Plated structural elements. European Committee for Standardization (CEN). 2006 [Online]. Available: https://www.phd.eng.br/wp-content/uploads/2015/12/en.1993.1.5.2006.pdf.
[2] prEN 1993-1-14:2020, Eurocode 3: Design of steel structures, Part 1-14: Design assisted by Finite element analysis (under development by Committee for Standardization (CEN)).
[3] Schillo N, Taras A, Feldmann M. Assessing the reliability of local buckling of plates for mild and high strength steels. J Constr Steel Res 2018;142:86–98. https://doi.org/10.1016/j.jcsr.2017.12.001.
[4] Schillo N, Taras A, Feldmann M. Assessment of safety factor for local buckling. WG5 Stuttgart 2016;26.
[5] Schillo N, Feldmann M. Local buckling behaviour of welded box sections made of high-strength steel: Comparing experiments with EC3 and general method. Steel Construction 2015;8(3):179–86. https://doi.org/10.1002/stco.v8.310.1002/stco.201510028.
[6] EN 1990. Eurocode 0: Basis of structural design. European Committee for Standardization (CEN); 2005. [Online] Available: https://www.phd.eng.br/wp-content/uploads/2015/12/en.1990.2002.pdf.
[7] Shi G, Zhou W, Bai Y, Lin C. Local buckling of 460 MPa high strength steel welded section stub columns under axial compression. J Constr Steel Res 2014;100:60–70. https://doi.org/10.1016/j.jcsr.2014.04.027.
[8] Clarin M. High strength steel: local buckling and residual stresses. Ph.D dissertation. Luleå tekniska universitet, Luleå,Sweeden ,2004. [Online]. Available: https://www.diva-portal.org/smash/get/diva2:990619/FULLTEXT01.pdf.
[9] EN 1993-1-1 (2005) (English): Eurocode 3: Design of steel structures - Part 1-1: General rules and rules for buildings. European Committee for Standardization

(CEN), 2005. [Online] Available: https://www.phd.eng.br/wp-content/uploads/2015/12/en.1993.1.1.2005.pdf.
[10] Nishino F, Ueda Y, Tall L. Experimental investigation of the buckling of plates with residual stresses. April 1966, 1966. https://doi.org/10.1520/STP43785S.
[11] Dwight J. Welded steel psates in compression. The Structural Engineering 1969;47:49–66.
[12] Rasmussen KJR, Hancock GJ. Plate slenderness limits for high strength steel sections. J Constr Steel Res 1992;23(1-3):73–96. https://doi.org/10.1016/0143-974X(92)90037-F.
[13] Bridge RQ, O'Shea D, M. Behaviour of thin-walled steel box sections with or without internal restraint. J Constr Steel Res 1998;47:73–91. https://doi.org/10.1016/S0143-974X(98)80103-X.
[14] Halme T, Huusko L, Marquis G, BjÖrk T. Local buckling of plates made of high strength steel. Proceedings of the 5th European conference on steel and composite structures, 2008, p. 3–5. [Online] Available: https://oxycoupage.com/FichiersPDF/Ruukki_Pdf/English/Ruukki-Technical-article-Local-buckling-of-plates-made-of-high-strength-steel.pdf.
[15] Schillo N. Local and global buckling of box sections made of High Strength Steel. Ph.D dissertation. RWTH Aachen University, Aachen, Germany,2017. [Online]. Available: https://publications.rwth-aachen.de/record/697419/files/697419.pdf.
[16] Von Kármán T. The strength of thin plates in compression. Trans ASME 1932;54:53–7.
[17] Winter G. Strength of thin steel compression flanges. Transactions of the American Society of Civil Engineers 1947;112(1):527–54. https://doi.org/10.1061/TACEAT.0006092.
[18] ANSYS® v17.2, Canonsburg, Pennsylvania, USA. [Online]. Available: https://www.ansys.com/.
[19] Yun X, Gardner L. Stress-strain curves for hot-rolled steels. J Constr Steel Res 2017;133:36–46. https://doi.org/10.1016/j.jcsr.2017.01.024.
[20] Gardner L, Yun X, Fieber A, Macorini L. Steel design by advanced analysis: material modeling and strain limits. Engineering 2019;5(2):243–9. https://doi.org/10.1016/j.eng.2018.11.026.
[21] Wang Y-B, Li G-Q, Chen S-W. The assessment of residual stresses in welded high strength steel box sections. J Constr Steel Res 2012;76:93–9. https://doi.org/10.1016/j.jcsr.2012.03.025.
[22] Khan M, Paradowska A, Uy B, Mashiri F, Tao Z. Residual stresses in high strength steel welded box sections. J Constr Steel Res 2016;116:55–64. https://doi.org/10.1016/j.jcsr.2015.08.033.
[23] Ban H, Shi G, Shi Y, Wang Y. Residual stress of 460MPa high strength steel welded box section: Experimental investigation and modeling. Thin-Walled Structures 2013;64:73–82. https://doi.org/10.1016/j.tws.2012.12.007.
[24] Degée H, Detzel A, Kuhlmann U. Interaction of global and local buckling in welded RHS compression members. J Constr Steel Res 2008;64(7-8):755–65. https://doi.org/10.1016/j.jcsr.2008.01.032.
[25] Somodi B. Flexural buckling resistance of high strength steel welded and cold-formed square closed section columns, PhD dissertation, Budapest University of Technology and Economics, Faculty of Civil engineering, Department of Structural Engineering, 2018. https://repozitorium.omikk.bme.hu/handle/10890/5517.
[26] EN 1090-2: 2018 - Execution of steel structures and aluminium structures - Part 2: Technical requirements for steel structures. European Committee for Standardization (CEN) 2016.